Agricultural and Forest Meteorology 256–257 (2018) 84–92

Contents lists available at ScienceDirect

Agricultural and Forest Meteorology

journal homepage: www.elsevier.com/locate/agrformet

The wind field in a cattle feedlot: measurements and simulations

J.D. Wilson[a,*], T.K. Flesch[a], S.M. McGinn[b]

[a] Department of Earth & Atmospheric Sciences, University of Alberta, Edmonton, Canada
[b] Agriculture and Agri-Food Canada, Lethbridge, Canada

ARTICLE INFO

Keywords:
Agricultural gas emissions
Cattle feedlot
Disturbed surface layer winds
Micrometeorology
Shelter
Windbreak
Wind model

ABSTRACT

Cup and sonic anemometers were operated in and about an empty pen (60 m × 68 m) on the outer (south) edge of a large cattle feedlot in southern Alberta. Mean wind speed, measured at constant height above ground, varied by more than a factor of four across the pen, the spatial transects being distinct for different wind directions—implying (for instance) that efforts to quantify feedlot gas emissions by micrometeorological methods will be prone to error, unless the drastic lateral inhomogeneity of wind statistics is accounted for. A subset of the observations, selected for southerly winds and weak thermal stratification, were aggregated and compared with steady-state, three-dimensional numerical simulations using "ASL3D", a Reynolds-averaged Navier–Stokes model with eddy viscosity closure that represents the influences both of feedlot windbreak fences and of topography (Wilson, 2018). Simulations confirm that wind drag on the tall ($H \approx 3$ m), low porosity (25%) slatted wooden fences was by far the dominant aerodynamic disturbance at this site. Various options were tested for the placement of computational domain boundaries, and it was found that the influence of fences at the faraway edges of *neighbouring* pens is practically negligible in comparison with that of the fences lying immediately upwind—that is, the transect of *relative* mean wind speed within the instrumented pen was largely determined by the nearest upwind fence(s). It is also concluded that when the mean wind is obliquely incident on low porosity fences of this type, simulations are improved if the horizontal wind component tangential to the fence is forced to vanish (at the fence).

1. Introduction

In western North America cattle feedlots experience a harsh winter climate, often motivating the provision of shelter for the animals (e.g. Bond and Laster, 1974; Dronen, 1988; Olsen and Wallander, 2002), and in western Canada this typically takes the form of a network of wooden slatted shelter fences bordering the pens. Scientists measuring the contribution of feedlots to methane (and other) budgets must therefore work in what is, from the micrometeorological perspective, a wind environment that could hardly be more different from the horizontal uniformity required if Monin–Obukhov similarity theory were to be posited as descriptive framework for the meteorology. This means, for instance, that if using eddy covariance the flux footprint would or could be very different from the available estimates, that invariably are based on a horizontally uniform wind regime. Similar difficulties attend the flux-gradient and the mass balance approaches, as well as the inverse dispersion approach (Denmead, 1995; Wilson et al., 2012) that is perhaps most widely used in the context of agricultural gas emissions.

Irrespectively of which micrometeorological method one may exploit for determining feedlot gas fluxes, correct application hinges on at least a qualitative assessment of the wind field, and if one were confident in being able to describe the wind regime quantitatively, there is the prospect of refining some of the available methods, e.g. one would be capable of computing the flux footprint over the feedlot, and put more generally, of bringing to bear a description of atmospheric transport attuned to the circumstances—correctly treating wind statistics as varying on all three spatial axes. Consequently it is pertinent to establish the potential accuracy of wind simulations of the feedlot environment, because it will never be feasible to quantify such a complex wind regime by measurement alone.

It is in this context, and in anticipation of pending inverse dispersion trials to measure cattle methane emissions differentially as a function of diet, that over an interval of a week we operated eleven cup anemometers and three sonic anemometers to monitor wind statistics in and about an empty pen on the outer edge of a cattle feedlot. In what follows we will describe the feedlot wind experiment, briefly outline a simple computational model of that flow, and compare the measured winds with model solutions.

* Corresponding author.
E-mail address: jaydee.uu@ualberta.ca (J.D. Wilson).

https://doi.org/10.1016/j.agrformet.2018.02.024
Received 19 January 2018; Accepted 20 February 2018
0168-1923/ © 2018 Elsevier B.V. All rights reserved.

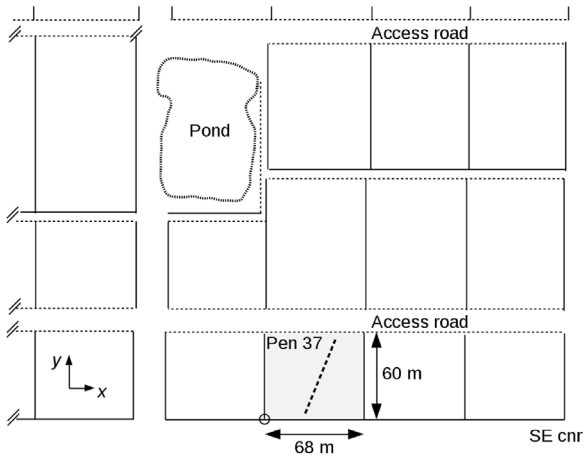

Fig. 1. Schematic of the southeast area of the feedlot (eastern-most five pens of the three southern-most rows). A further nine rows of pens stood further north, while a further three columns of pens stood west of those shown. Sketch is approximately to scale, but gateways have not been shown. Solid lines are windbreak fences (height ~3 m), while light dashed lines are low stock barriers fabricated in steel pipe: these offered minimal impediment to the wind. Narrow alleys are stock routes. The coordinate origin, at the SW corner of pen 37, is shown by a circle. The heavy dashed line in pen 37 identifies the cup anemometer transect.

2. Experiment

The experiment took place 11–18 July 2017 at a prairie cattle feedlot (approximately 1 km × 1 km in areal span) a few kilometers from Nanton (Alberta, Canada). Pen 37, which for the purposes of the experiment was emptied of cattle, lay at the south edge of the feedlot, and not far from its south-east corner (see Fig. 1): it was flanked to its east by two and to its west by more numerous occupied pens. Figs. 2 and 3 give a view of pen 37, and the instrument layout: it can be seen that the amplitude of the topography across the pen was very modest, as confirmed by the elevation contours of Fig. 4. In this paper the coordinate system has been aligned with the fences of the pens, the origin $(x, y) = (0, 0)$ lying in the SW corner of pen 37 (at the farther end of the gate visible in Fig. 2). The alignment of the (nominally) east-west running fences (thus, the x-axis in this paper) deviated by only 3.4° from latitude lines, and pen 37 spanned distances $(X, Y) = (68, 60)$ m on respectively the (x, y) axes.

More than 50 m south of pen 37 and the feedlot as a whole, lay two small (lateral span ~5–10 m), low (height ~2–3 m), weed-covered hillocks of material scraped from the pens, while to the south-west at a distance of at least 150 m from pen 37 a berm (height ~3 m) surrounded a water reservoir. These features were not represented in the wind simulations to be described below.

Seven cup anemometers (Climet, Inc., 011-4) were disposed (at height above ground $\eta = 1.15$ m) along a line crossing pen 37 obliquely, at the positions given in Table 1. A further four Climet cup anemometers measured the profile of mean wind speed on a 6 m mast near the N end of pen 37. Two 3-dimensional sonic anemometer-thermometers (Campbell Scientific Inc., CSAT3) were operated within the pen, always at $\eta = 2$ m. One was mounted on the mast, the other sited either near the middle ('mid', $y \sim Y/2$) of pen 37, or near $y \sim Y/4$. A further CSAT3 sonic was operated south of the south boundary of pen 37. Table 1 gives the coordinates of all instruments.

Shelter fences, forming a network about the feedlot, bounded pen 37 on the west, south and east sides, and were composed of vertical wooden slats of cross-section 9.5 × 1.1 cm ($3\frac{3}{4} \times \frac{7}{16}$ in) with an average gap space of 4.4 cm ($1\frac{3}{4}$ in), the resulting porosity being 25%. The height of the shelter fences relative to ground varied somewhat, and was determined at 10 m intervals. For the purpose of the simulations below each fence was attributed a constant height. The south boundary fence ($H_S = 2.9$ m) ran along the entire $y = 0$ axis (excepting the interval $0 \le x \le 8$ m, the opening for the SW gate). The west fence ($H_W = 2.4$ m) ran northward (only) along $x = 0$, and the east fence ($H_E = 2.65$ m) northward along $x = X = 68$ m. At its north edge, pen 37 was bounded only by a low concrete berm and a highly porous steel pipe fence (see Fig. 3), whose aerodynamic effect (over pen 37, during southerly winds) has been assumed negligible.

A Campbell Scientific Inc. (CSI) CR7 datalogger averaged the cup anemometer windspeeds over 15 min intervals, while each sonic anemometer was equipped with a CSI CR10X logger computing mean wind and turbulence statistics over the same 15 min intervals.

2.1. Data analysis

In order to aggregate the mean wind speeds, and in order (also) to allow comparison of measured and computed fields, it was necessary to choose a reference wind speed from a single instrument and normalize using that value. Here the uppermost instrument ("T4", at 5.08 m above ground) on the mast near the N end of pen 37 has been used, thus S/S_{T4} denotes a normalised mean wind speed. (Note: to a first approximation, cup anemometer overspeeding error cancels out in these *ratios* S/S_{T4} of mean speeds; e.g. Wilson (2004a,b).)

A Fortran program aggregated the anemometer data for wind direction sectors of angular width ± 10° or ± 15° about the SE, S and SW compass directions; this narrow sector width was chosen because shelter flows within windbreak networks exhibit a strong "corner effect" (e.g. Wilson and Flesch, 2003); results were not very different, however, with wider ± 22.5° sectors. To avoid periods when one or more anemometers may have intermittently stalled, any run with $S_{T4} < 1.5$ m s^{-1} was discarded, and a further criterion on the Obukhov length L was imposed (the latter was deduced from the north sonic anemometer, and can be interpreted only as being *broadly* indicative of the prevailing stratification).

Fig. 2. View towards (roughly) the SSW across pen 37. Transect of seven cup anemometers all at $\eta = 1.15$ m above ground level (referred to in the text by number, no. 7 being the closest to camera). Anemometer no. 5 stood some 0.8 m below the mean level of the plot. Beyond the gate in the SW corner of the pen can be seen higher ground: the nearby berm of a feedlot reservoir, and (barely distinguishable) the foothills some 20–30 km distant.

Fig. 3. View towards (roughly) the NNE across pen 37 (cup anemometer no. 1 out of view). The uppermost cup anemometer on the mast ("T4") stood 5.08 m above ground. Note the sonic anemometer on the left-most tripod, matched in height to another on the 6 m tall, triangle-section mast.

Table 1
Anemometer positions, and, measured transects and profiles of normalized mean wind speed S/S_{T4} in (SE, S, SW) winds averaged over $n = (25, 11, 12)$ runs (respectively). Selection criteria for the transects and profiles: wind direction sector width ± 10°, Obukhov length $L \leq -40$ m and $S_{T4} \geq 1.5\,\mathrm{m\,s^{-1}}$ (weakly unstable stratification).

Instrument	x [m]	y [m]	z [m]	SE	S	SW
A1	27.8	5.0	1.15	0.26	0.16	0.19
A2	30.4	11.4	1.15	0.52	0.30	0.54
A3	32.6	16.9	1.15	0.64	0.36	0.63
A4	35.0	23.3	1.15	0.71	0.41	0.68
A5	39.5	34.0	1.15	0.71	0.54	0.72
A6	44.2	45.4	1.15	0.70	0.71	0.78
A7	48.2	54.7	1.15	0.67	0.82	0.82
T4	37.2	56.0	5.08	1.00	1.00	1.00
T3	37.2	56.0	3.12	0.88	0.90	0.91
T2	37.2	56.0	1.66	0.80	0.80	0.84
T1	37.2	56.0	0.66	0.70	0.75	0.77
North sonic	37.2	56.0	2.0			
Mid sonic	31.6	30.8	2.0			
South sonic	45.5	17.6	2.0			
Upwind sonic	−9.0	−67.3	5.53			

3. Numerical simulation of the wind field

A simple numerical model ("ASL3D"), previously described and tested by Wilson (2018), was used to simulate the wind field over the feedlot. This is a RANS (Reynolds-Averaged Navier–Stokes) model using an eddy viscosity closure. The flow response to topography (and windbreaks) is computed in a terrain-following coordinate system (x, y, η) on a laterally-periodic domain, the eddy viscosity being computed as $K = \lambda\sqrt{c_e E}$ where $E = E(x, y, \eta)$ is the computed turbulent kinetic energy, c_e a dimensionless closure constant, and $\lambda = \lambda(\eta)$ an imposed, laterally-invariant turbulence length scale.

The vertical coordinate is $\eta = D(z - h)/(D - h)$, where $h = h(x, y)$ is the ground elevation and D is the model's domain depth. The host flow (to which the solution conforms in the absence of any disturbance) is a deep constant stress layer (i.e. undisturbed atmospheric surface layer), and any effect of thermal stratification is neglected; accordingly, and because the length scale was not adjusted to represent any response to the shelter fences, near ground the turbulence length scale goes as $\lambda = k_v\eta$ where k_v is the von Karman constant. Further details are given in Appendix A (and in Wilson, 2018).

3.1. Model domain

Because ASL3D treats all lateral boundaries as periodic, pen 37 occurs not in isolation but in infinite repetition. Nevertheless by arranging that the computational domain embrace an open area outside pen 37, it is possible to at least partially "isolate" pen 37 (aerodynamically) from those periodic images of itself. For brevity the horizontal span of the domain will be referred to in the format $[x_1{:}x_2]$ $[y_1{:}y_2]$, implying it encompassed $x_1 \leq x \leq x_2$, $y_1 \leq y \leq y_2$. All lengths will be given in [m], and specific examples for which results will be shown are:

- $D_{\mathrm{I}} = [0{:}X][-120{:}120]$
- $D_{\mathrm{II}} = [-X{:}X][-120{:}120]$
- $D_{\square} = [-120{:}180][-120{:}180]$

where (recall) $X = 68$ m is the width of pen 37. Unless otherwise noted, domain *depth* was $D = 380$ m.

Simulations were also carried out on several other domains, notably, domains of larger depth (e.g. $D = 480$ m) or with larger lateral span $[-180{:}180][-180{:}180]$, and some simulations explicitly represented not only the fences bounding pen 37 on its (E,W,S) sides, but also the distant N fence ($y = 168$ m), and, the north-running fences bounding adjacent pens to the east and west of pen 37. Results from these simulations are not shown because the outcomes lay within the compass of those furnished on domains D_{I}, D_{II} and $D_{\square}$.

It is evident from the pen 37 elevation contours (Fig. 4) that ground elevation transects along the east and west boundaries of pen 37 were

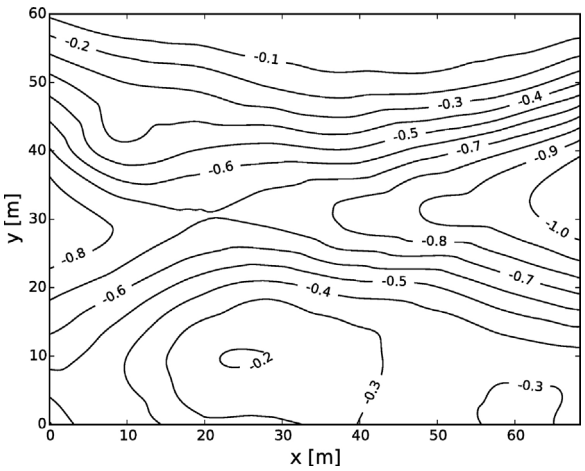

Fig. 4. Relative topography of pen 37 with 0.1 m contour interval, constructed from a survey grid with 10 m horizontal resolution. For modelling purposes, ground elevation was relaxed to zero away from the edges of the pen over a distance of 1 km, such that the effective slope outside the pen was negligible.

not identical, so that domain D_I entails small height discontinuities across its east and west boundaries.[1] It will be seen that those discontinuities of elevation exerted little effect, and that topographic forcing of the feedlot wind field was much less important than windbreak drag.

3.2. Treatment of fences

In the case that the mean wind encounters a thin porous barrier at perpendicular incidence, the dimensionless parameters controlling the disturbed wind field are, in order of decreasing importance, the resistance (or "pressure loss") coefficient k_r of the fence, and the ratio H/z_0 of fence height to the surface roughness length (Wilson, 1985). For a barrier composed of sharp-edged strips and having 25% porosity, Hoerner's (1965; Ch. III Sec. 9; Eq. (49) & Fig. 43) correlation gives the pressure loss coefficient as

$$k_r = \frac{\Delta P}{\rho U^2} = 12.5, \tag{1}$$

where ΔP is the pressure drop across the barrier if it were mounted perpendicularly so as to block a laminar, unsheared airstream of speed U and density ρ. This is the value adopted for all the of the wind simulations to be shown below.

Consider now a section of pen 37's western border fence (running along $x = 0$ at $y \geq 0$). In the ASL3D model the impact of this fence on the perpendicular wind component U can be parameterized by adding a momentum sink S_U to the right hand side of the U-momentum equation (i.e. Eq. (A.1) in Appendix A), viz.

$$S_U = -k_r U|U|\delta(x-0)u(y-0)u(H_W - \eta). \tag{2}$$

Here the delta-function $\delta(x-0)$, having the unit $[m^{-1}]$, localizes the drag to $x = 0$, and $u(\cdot)$ is a dimensionless unit step function, further localizing the drag to non-negative values of its argument (i.e. here to $y \geq 0$ and $\eta \leq H_W$). Eq. (2) assumes (Wilson, 2004a,b) "that it is the normal component of the wind that controls the pressure loss across the fence", and unless otherwise stated this is the formulation employed; a few simulations will also be shown for which drag on the normal component was treated as being proportional to $U\sqrt{U^2+V^2}$ rather than $U|U|$, and these will be identified by the notation $\measuredangle$, signifying that a force proportional to $(U^2 + V^2)$ has been projected onto the direction normal to the barrier.

Eq. (2) exemplifies the drag exerted on the *normal* component of the wind, but what of the impact upon the *parallel* component (in this case, i.e. the west fence, the component V)? In the context of a mean wind incident obliquely on a long straight fence (composed of 45% porous, plastic screen), Wilson (2004b; Sections 2b; 5b) experimented with several treatments, regarding it as simplest to entirely neglect any influence of the barrier on the component tangential to it ("free slip"). Here however it will be seen that, for the present type of fence at least, it is advantageous to require that *the horizontal mean wind component parallel to a fence must vanish "at" the fence*, i.e. simulations that impose a no-slip condition on the horizontal velocity component tangential to the fence are demonstrably superior. With the exception of cases identified by "fs" (for "free slip"), all model solutions shown below *have* imposed the no-slip condition (on horizontal components parallel to barriers).

Finally, what of the effect of the barriers on turbulent kinetic energy (TKE)? It has been known at least since the work of Raine and Stevenson (1977) that there is a ground-based "quiet zone" of reduced turbulence in the immediate wake of a (porous) windbreak, but that a turbulent wake spreads downwind from the enhanced wind shear zone near the top of the obstacle. Representation of a quiet zone can be enforced (Wilson, 1985, 2004a,b) by adding a TKE sink to the right hand side of Eq. (A.4), e.g. to represent the west fence, running along $x = 0$ at $y \geq 0$, the sink is

$$S_E = -k_r E|U|\delta(x-0)u(y-0)u(H_W - \eta). \tag{3}$$

A wake zone occurs spontaneously in the simulations because enhanced mean velocity gradients in the region of the barrier result in enhanced shear production.

4. Results and discussion

Fig. 5 gives aggregate profiles of normalized mean wind speed S/S_{T4}, measured on the mast near the N. end of pen 37, for SE, S and SW wind directions (see also Table 1), and in addition, two profiles from ASL3D—from which mean wind speed was evaluated as[2] $S = \sqrt{U^2 + V^2}$, and re-normalised on its value S_{T4} at the location of anemometer T4. This mast is *not* situated in an undisturbed flow so it is not surprising that the measured profiles should depart, as they evidently do, from being semi-logarithmic. Neither is it surprising that the apparent roughness length, if deduced from the lower pair of anemometers, should be smaller than that implied by the uppermost pair—for (loosely speaking) the footprint affecting the lower anemometers is the smooth surface of the pen, while higher on the tower some influence of the wake of the fences could be expected to affect the mean shear.

There are two points to be made. Firstly, some ambiguity surrounds the proper value of the surface roughness length z_0 for the wind simulations to follow; except where otherwise specified, simulations used $z_0 = 0.005$ m, and in any case they proved not to be very sensitive to the choice. Secondly, it cannot be assumed that the normalizing wind speed S_{T4} at 5.08 m AGL represents the speed at that height upwind from the feedlot; the choice of T4 as normalizing speed represents what one might call an "internal" reference speed, in the sense that the chosen point lies within a disturbed flow.

The solid black line in Fig. 5 confirms that ASL3D's equilibrium wind profile $S_0(z)$ (no fences, no topography) is (as per design) semi-logarithmic,[3] and that ASL3D's solution for the (disturbed) wind profile at the mast in a south wind, taking into account both fences and topography, is (as expected) *not* a semi-logarithmic profile (blue dashed line in Fig. 5). The model profile at the mast shows the correct shear aloft, but a stronger shear at small heights (and larger apparent roughness length) than the measured profile.

Fig. 6 shows the transect of mean wind speed across pen 37 during south winds, for unstable, approximately neutral, and stable stratification. Focusing first on the neutral case (which is of most interest because the numerical model ASL3D treats the atmosphere as neutral), the pattern is little different whether the acceptance angle for mean wind direction is 180 ± 10° or a wider 180 ± 15°, and neither does the pattern change very noticeably depending on whether an additional 14 runs having $-80 \leq L \leq -40$ m are added to those satisfying $L \leq -80$ m. Fig. 6 also conveys the impact of strong stratification, unstable or stable, on the transect of mean wind speed. For the case of stable stratification the dip in relative wind speed at anemometer no. 5 (situated in the hollow of the pen) may owe to intermittent stalling of the cup (strengthening the acceptability criterion on S_{T4} from 1.5 m s^{-1} to 2.5 m s^{-1} lessens the dip, but even the stronger criterion may not have excluded periods when anemometer A5 stalled). Fig. 6 testifies to the fact that the wind field is *extremely* inhomogeneous: over pen 37 the mean wind speed varies by more than a factor of four, emphasizing that

[1] In truth there *were* some height discontinuities from one side of a fence to another.

[2] In ignoring the contribution of horizontal velocity *fluctuations* to the mean speed, this definition of the latter is distinct from the mean speed furnished by cup anemometers. One could have invoked a correction based on the model's TKE field, but again, to a first approximation that correction would have (at most) a minor effect on model wind speed *ratios*.

[3] This hinges on making a sufficiently small choice for the artificial viscosity K_a^v (see Appendix A).

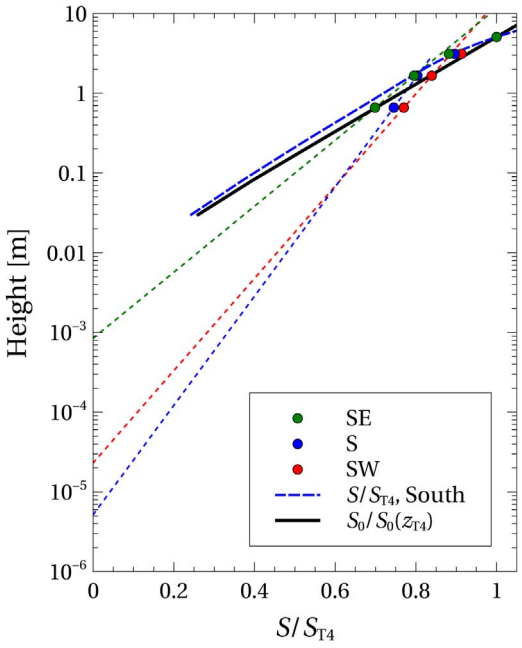

Fig. 5. Profiles of normalised mean wind speed, on the mast near the N end of pen 37, for SE, S and SW mean wind directions. Selection criteria $L \leq -40$ m, $S_{T4} \geq 1.5$ m s^{-1}. The coloured straight short-dashed lines give the slopes defined by the lowest two points of the (corresponding) measured profile, and imply an *apparent* surface roughness length (z_0). The black solid line is the ASL3D *equilibrium* solution (i.e. no disturbance: no topography and no fences) for the choice $z_0 = 0.005$ m (used in most simulations), while the blue long-dashed curve is the ASL3D solution for the profile at the mast in a south wind, accounting for topography and fences (and again, with $z_0 = 0.005$ m). (For interpretation of the references to colour in this figure legend, the reader is referred to the web version of the article.)

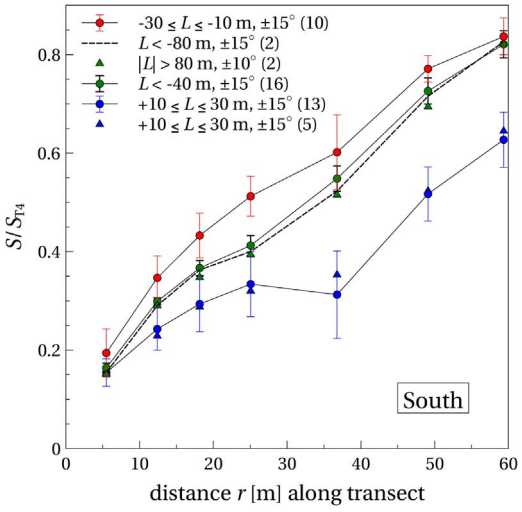

Fig. 6. Measured transects of normalised mean wind speed as a function of stratification, for south winds (distance r is measured along the line of the transect, starting where it would intersect the south fence). Symbols give mean and (±) standard deviation over n intervals (n given in brackets). The threshold wind speed was $S_{T4} \geq 1.5$ m s^{-1}, except for the triangular blue symbols for which $S_{T4} \geq 2.5$ m s^{-1}.

implementation of a standard micrometeorological flux technique that presupposes horizontal homogeneity of the wind and turbulence fields would be likely to yield inaccurate conclusions.

4.1. Comparison of simulations with measured mean winds

From an aerodynamic perspective the case of a south wind over pen 37 is expected to be simplest, for here the wind approaches the nearest

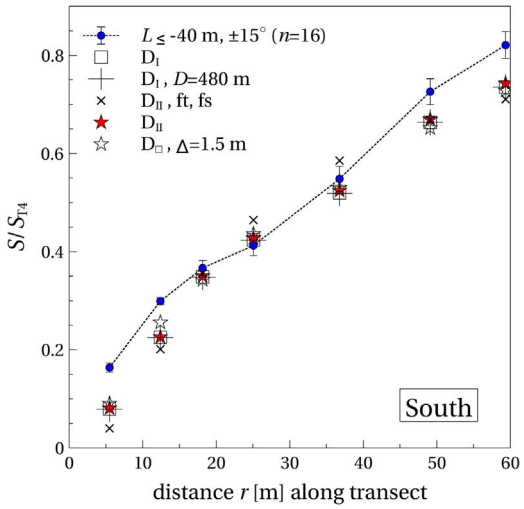

Fig. 7. Measured and modelled transects of normalised mean wind speed, for south winds and neutral stratification. For the observations the reference wind speed was required to satisfy $S_{T4} \geq 1.5$ m s^{-1}. Error bars give ± the standard deviation over the sample of n runs. For the simulations "ft" signifies flat terrain, and "fs" signifies free slip of the wind component parallel to a fence (absence of that notation implies that the "no slip" condition was applied to the horizontal component parallel to each windbreak). Where not otherwise specified, horizontal resolution $\Delta = 0.75$ m (i.e. $H/4$) and domain depth $D = 360$ m.

upwind (and therefore, most important) windbreak at *normal incidence*. The measured pattern (under neutral stratification) is reproduced in Fig. 7, in comparison with the results of several simulations.

As regards the latter, please note that *at no point* on the transect have the modelled and measured relative wind speeds been forced into agreement, and that (as for all simulations shown) the resistance coefficient imposed ($k_r = 12.5$) is that given independently by Hoerner's tabulation. Therefore although Fig. 7 demonstrates a band of outcomes from the model depending on particular choice of domain and gridlength, the bigger story is that the more than fourfold variation of mean wind speed over the pen has been simulated rather well. Note that a simulation that does not account for the pen topography (black crosses) yields a montonic decay in the rate ($\partial S/\partial r$) of recovery of mean wind speed, whereas simulations that include topography show a less regular recovery that accords better with the observed transect. It is understandable that for this case of a south wind, the component U tangential to the most important (i.e. south) fence being small, it is of no consequence whether or not a no slip condition is imposed on velocity components tangential to fences. Overall we can conclude from Fig. 7 that the simulation is in tolerably good agreement with the observed transect, and that the principal aerodynamic disturbance stems from the south fence, the topographic irregularity superposing its own smaller signature. If, furthermore, variations of topography and cover standing (broadly) upwind from the south fence have at all influenced the measured transect, their effects, not accounted for in the simulation, must have been secondary to windbreak drag. Computed transects with domain depths $D = (360,\ 480)$ m are indistinguishable. The configuration associated with the red stars in Fig. 7 will be referred to as the "standard" configuration (D_{II}; $\Delta = 0.75$ m; topography included; no slip condition imposed on tangential component parallel to fence; pattern of Eq. (2) for drag on normal components).

Fig. 8 gives measured and modelled transects of mean wind speed for the case of a south-east wind, and (nominally) neutral stratification. Concerning the observations, note that the pattern does not greatly depend on the inclusion or rejection of runs having $-80 \leq L \leq -40$ m, and nor does a widening of the sector of acceptable mean wind directions (from ± 10° to ± 15°) appreciably affect the observed pattern. The northern end of the anemometer transect trends towards the eastern shelter fence (at $x = X \equiv 68$ m), such that in the case of a SE

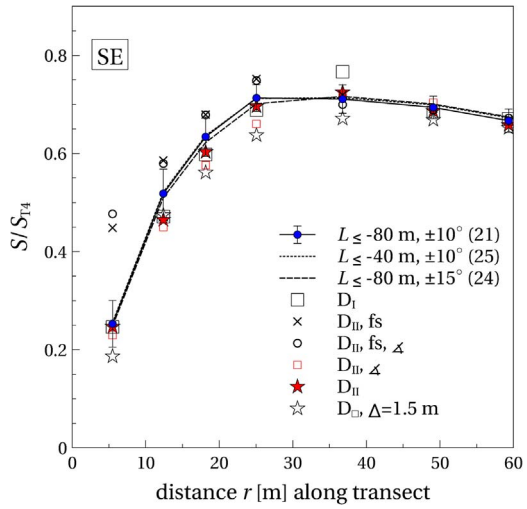

Fig. 8. Measured and modelled transects of normalised mean wind speed, for south-east winds and neutral stratification. Notation and legend as for Fig. 7. The symbol ⊿ signifies that drag on wind components perpendicular to fences, rather than being specified on the pattern of Eq. (2), was set proportional to the projection of $(U^2 + V^2)$ onto the normal.

wind the northern-most anemometer (no. 7) is to some extent sheltered. This explains why Fig. 8 indicates higher relative wind speeds at cup nos. (4,5,6) than at cup no. 7.

The simulations shown in Fig. 8 all imposed a momentum sink on the normal wind component at any fence, and as the figure indicates, imposing the no slip condition on the wind component *parallel* to any fence is decisively advantageous. Furthermore treatment of fence drag on the perpendicular component (say, U) as being proportional to $U|U|$ yielded a slightly better simulation than if it were set proportional to $U\sqrt{U^2+V^2}$ (for the case of a SW wind however, there was no significant difference in this respect). Simulated transects do vary slightly from one choice of domain to another, and simulation on the "standard" domain (D_{II}) with its lateral span $[-X:X]$ emerges as being marginally superior to the narrower D_I spanning $[0:X]$, and in excellent agreement with the observations.

For south-west winds (Fig. 9) it is once again the case that imposition of the no-slip condition on the horizontal wind component parallel to fences results in a markedly improved simulation. It is interesting that the transects for south-west winds differ from those produced in south-east winds. This asymmetry arises from a combination of the following factors: (a) as is evident from Fig. 1, the

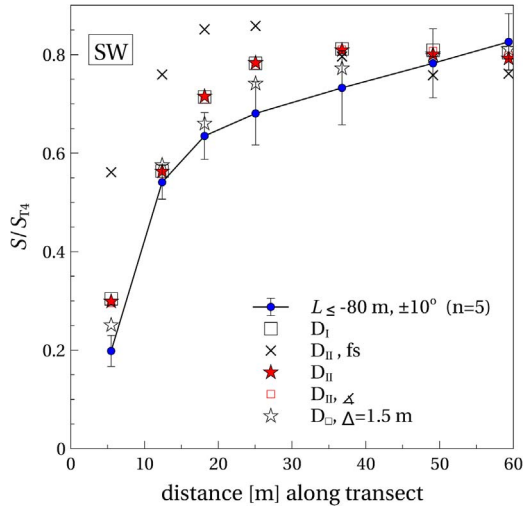

Fig. 9. Measured and modelled transects of normalised mean wind speed, for south-west winds and neutral stratification. Notation as for earlier figures.

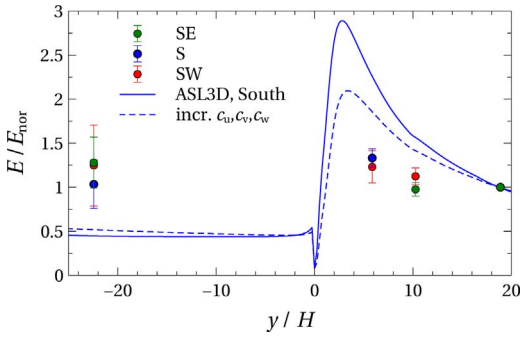

Fig. 10. Transects of normalized turbulent kinetic energy at $\eta/H \approx 2/3$, for SE, S and SW wind directions. TKE has been normalized by the value on the mast at the north end of pen 37, so that all transects run through unity at that point and measurement symbols for the S and SW cases are masked: error bars (elsewhere) give ± the *standard error* (not, as on other figures, the standard deviation). Acceptance criteria: $L \leq -40$ m, mean wind direction 180 ± 10°, and $S_{T4} \geq 1.5\,\mathrm{m\,s^{-1}}$. Measurement height at the upwind location was 5.53 m, whereas the sonic heights in the pen were 2 m (no height correction has been applied). The blue lines show ASL3D solutions for the TKE transect in south winds (domain D_{II}, horizontal gridlength $\Delta = 0.75$ m). The solid line corresponds to the "standard" mean wind speed solution given in Fig. 7 by solid red stars; the simulation indicated by the dashed line differs only in that the closure constant c_e has been evaluated using larger values for (c_u, c_v, c_w), viz. (2.5, 2.5, 1.6). (For interpretation of the references to colour in this figure legend, the reader is referred to the web version of the article.)

anemometer transect ran obliquely across pen 37, so that the distance of any cup anemometer from the west fence differed from its distance from the east fence; (b) the west fence was slightly lower than the east fence; (c) only two (occupied) pens stood east of pen 37, while five or more lay west; and finally, (d) the topography upwind of pen 37 differed for SE and SW winds. Only factors (a,b) were accounted for in the simulations, but this degree of fidelity evidently suffices to model the distinctively different character of the SE and SW transects.

Concluding this section, Figs. 7–9 have shown that ASL3D, despite its being an exceedingly simple treatment, computes the relative mean wind speed almost everywhere[4] over pen 37 to within an error of no worse than about 20%. Given the more than fourfold variation of wind speed about the pen, this amounts to a significant improvement over merely treating the mean wind speed as horizontally-uniform (as would be the case were one to invoke the Monin–Obukhov description).

4.2. Turbulence pattern in the feedlot, and its simulation

In the context of inverse dispersion (which necessitates modelling turbulent transport in the feedlot) the spatial pattern of turbulence is (in principle) no less important than the pattern of the mean wind. Fig. 10 gives a transect of turbulent kinetic energy measured (albeit sparsely) across the feedlot by the sonic anemometers, those in the pen having been placed at $x \sim 30$–40 m (roughly along the centreline of the pen) at height $\eta/H \sim 2/3$ (the same instrument sampled the mid and south stations in the pen, at different times). For each sonic anemometer, a coordinate rotation was applied to make the apparent mean vertical velocity vanish, but the turbulent kinetic energy E is indifferent to that rotation.

Focusing on the simplest case, in a south wind the TKE roughly $6H$ downwind from the S. fence was elevated by about 30% relative to upstream (the greater height of the upwind sonic than those in the pen would if anything suggest a TKE enhancement in the lee of the fences that exceeds 30%). Also shown in Fig. 10 are two ASL3D transects of (normalized) TKE corresponding to south winds, differing only in their specification of the closure constant c_e (which is fixed by one's choices of $c_u = \sigma_u/u_*$ etc., the normalized velocity standard deviations, in

[4] Fractional error of the modelled wind transect is greater close to the south fence, where the absolute mean wind speed is smallest.

undisturbed surface layer flow). The degree of enhancement of TKE in the wake zone is excessive relative to the modest enhancement (circa. 30%) indicated by the measurements—although reminiscent of Wilson's (1985, Fig. 14) model transect of streamwise velocity variance.

Interpreting this disparity between the amplitudes of the modelled and measured TKE transects at the feedlot necessitates the provision of some context. There have been few full scale measurements of turbulent kinetic energy around a windbreak. Probably the most comprehensive field data are those reported by Finnigan and Bradley (1983, Fig. 3), taken in neutrally-stratified winds encountering a 50% porous fence at perpendicular incidence. Finnigan and Bradley's transect of TKE along a streamline passing the tip of the barrier shows that TKE in the near wake ($x/H = 5$) had increased more than twofold relative to the upwind value at the same height, while along the streamline through $z/H = 1/2$ the fractional increase was even larger—much larger than seen in our present (but much less comprehensive) transect along $\eta/H \sim 2/3$. Wilson's (1987) field measurements in a broadly similar flow (weakly stratified, and encountering a straight 50% porous fence at nearly perpendicular incidence) showed that σ_w^2 may be enhanced by almost a factor of 3 along $z/H = 1$ (TKE was not reported, as the single axis sonic anemometers employed could not measure the streamwise velocity variance). Subsequent measurements by Wilson (2004a,b) with 2- and 3-dimensional sonic anemometers suggested fractional increases in the *horizontal* velocity variances in normally-incident winds are more modest, roughly 10-20%. This latter result is broadly consistent with those of Jacobs and Wartena (1987), who used cup anemometers, arrayed about an isolated *solid* fence, to comprehensively map the pattern in the standard deviation of horizontal wind speed (σ_u/σ_{u0}, where σ_{u0} denotes the value at the same height, far upwind); their results, covering the variation of σ_u/σ_{u0} versus height, downwind distance, angle of approach and thermal stratification, suggest that along $z \sim H$ (and excluding periods of strong stratification) the increase in horizontal velocity variances relative to upstream is quite modest, say ~20%. Extrapolating on the basis that (at least in undisturbed flow) the horizontal velocity variances handily exceed vertical velocity variance, one might anticipate that the changes in TKE in windbreak flow will be determined to a much greater extent by changes in (σ_u^2, σ_v^2) than by changes in σ_w^2.

A wind tunnel and Large Eddy Simulation (LES) study (Judd et al., 1996; Patton et al., 1998) complements the few field studies of turbulence changes in windbreak flow. Patton et al. (1998 give contours of TKE computed by LES for a periodic array of porous windbreaks (height H, separation $12H$) extending above a "wheat" canopy (of height $H/3$). A zone of increased TKE was centred at about ($x/H = 6$, $z/H = 1$), however the maximum value for TKE in that location was only some 20% larger than the (rather uniform) upstream value. Complicating the interpretation here, is the fact that the periodicity of the LES flow implies that the "upstream" region of the windbreak is also downstream: and that the array as a whole would have produced an enhanced level of turbulence relative to that which would be found in the same flow upwind of all obstacles (Judd et al., 1996). Patton et al. (Figs. 5,6) also show profiles of streamwise and vertical velocity variances, both for their LES and for the wind tunnel study of Judd et al. Focusing on the wind tunnel data, there is no sign of anything like a 300% increase in σ_w^2.

Returning to Fig. 10 armed with this overview, we conclude that the TKE pattern measured at the Nanton feedlot is roughly in line with Jacobs and Wartena (1987) and with the LES outcome. By the criterion of these measurements the TKE simulation produced by ASL3D is unrealistic, despite the good model outcome as regards computed mean wind speed. If this seems an intrinsic contradiction, it can perhaps be comprehended as follows: firstly, note that in these simulations the TKE field affects the wind speed field only by the mediation of the eddy viscosity, which is proportional to the *square root* of the TKE (a 100% error in model TKE produces only a 50% error in eddy viscosity); and secondly (and probably more importantly, in this case), whereas the primary impact of the eddy viscosity in the mean velocity calculation is to compute the divergence of the shear stress fields, strong mean pressure gradients induced in windbreak flow imply that (except far from the fences) the shear stress gradients are not necessarily paramount terms in the momentum budget.

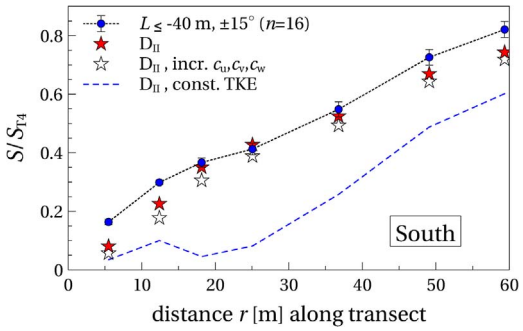

Fig. 11. Measured and modelled transect of normalised mean wind speed, for south winds: comparing 'standard' simulation (solid red stars) versus simulations with increased (c_u, c_v, c_w) or with spatially-invariant turbulent kinetic energy E. (For interpretation of the references to colour in this figure legend, the reader is referred to the web version of the article.)

The TKE equation used by ASL3D is (by design) very simple. Fig. 11 however, giving the standard model wind transect (red stars) along with one in which TKE is held constant, proves that including a TKE equation, even if imperfect, is much better option than merely treating the turbulent kinetic energy as invariant[5] (and by implication, the eddy viscosity as undisturbed). Certainly it is to be hoped that a better formulation can be worked out, e.g. by heuristically refining the specification of the TKE dissipation rate (here $\epsilon \propto E^{3/2}/\lambda$ with length scale λ unaffected by the disturbance) and/or the turbulence length scale (Wang et al., 2001); it would be helpful if more comprehensive experimental guidance were available than presently exists.

5. Conclusions

Beyond documenting the non-uniformity of winds across this feedlot, a feature unlikely to surprise those familiar with windbreak effects, the main novelty of this paper is its finding that thin, low porosity windbreaks of the type encountered here are better represented computationally when, in addition to imposing drag on the *perpendicular* wind component "leaking" through the barrier, the *tangential* component is subjected to the "no-slip" condition (i.e. forced to vanish at the barrier). Apart from the flexibility implicit in that choice, and the arbitrariness intrinsic to having chosen a particular turbulence closure, the wind simulations reported above are objective: the geometry of the fences and the topography of the pen are known; the primary aerodynamic characteristic of the fence material (its resistance coefficient k_r) has been deduced without freedom from a classic engineering correlation; the surface roughness length (thus, ratio H/z_0 of fence height to roughness) is somewhat uncertain, but, it is well established that windbreak flows are not very sensitive to this ratio; the numerical method used by ASL3D is a standard one; and finally, an exhaustive series of trials with differing domains and differing grid resolution has established that the model transects, while not absolutely indifferent to further refinement in those respects (wider domain, finer resolution) are as close to being so as matters here. Numerical solution of the Reynolds equations is clearly a promising basis for determining the spatial variation of wind statistics in the complex environment of a feedlot.

It would seem from Section 4.2 that the gravest weakness of ASL3D

[5] This may seem something of a paradox, because Fig. 10 reveals the observed TKE transect as being closer to a flat line (constant) than to the model transect.

is its simplistic turbulent kinetic energy equation—and given the importance of the turbulent velocity scales ($\sigma_{u,v,w}$) for atmospheric dispersion and the ambiguity (covered in Section 4.2) as to their true variation about windbreaks, further experimental transects about a variety of types of windbreak would be helpful. That the impact of shelter fences on the TKE field should be more difficult to capture than their impact on mean wind speed is understandable: the mechanism for mean wind reduction is simple and (accordingly) well represented, viz., by a localised momentum sink that results in strong horizontal pressure gradients that *lessen* the relative importance of the (imperfectly represented) turbulent shear stress divergence; but in contrast, the TKE disturbance is accompanied by a difficult-to-model disruption of the velocity power spectrum (or simplistically put, the eddy length scale) and therefore a disturbance to the TKE dissipation rate ϵ (see Eq. (A.4)), a distributed TKE sink.

Lastly, it is interesting that realistic mean wind simulations have been obtained from calculations encompassing only small, periodic domains (D_{I}, D_{II}) that extend little (if at all) beyond the confines of the instrumented pen, suggesting that a description of the feedlot wind field by Large Eddy Simulation (LES) should be computationally practicable. Though it would remain necessary to parameterize the fluctuating drag on fences (because resolving the intricate motion through pores remains unthinkable), by explicitly resolving the larger eddies LES might remedy the weakest element of the RANS approach.

Acknowledgments

The authors thank Mr. Rick Sears and Mr. Mike Pollard for having kindly permitted our access to the feedlot. We also thank Dennis Lastuka (AAFC, Lethbridge) for assistance with the field work. This work has been funded by Emissions Reduction Alberta, by the Agricultural Greenhouse Gases Program (AGGP) of Agriculture and Agrifood Canada, and by the Natural Sciences and Engineering Research Council of Canada.

Appendix A. Wind model ASL3D

In the terrain-following (x, y, η) coordinate system the U-momentum equation is

$$\frac{\partial}{\partial x}\left(\mathrm{UU} - K_a^h \frac{\partial U}{\partial x}\right) + \frac{\partial}{\partial y}\left(\mathrm{VU} - K_a^h \frac{\partial U}{\partial y}\right) + \frac{\partial}{\partial \eta}\left(W^* U - \eta_z^2 K \frac{\partial U}{\partial \eta}\right) = -\frac{\partial P}{\partial x} - \eta_x \frac{\partial P}{\partial \eta} \tag{A.1}$$

where P is the mean kinetic pressure field induced by the flow; K is the eddy viscosity; $\eta_z = D/(D-h)$; and $W^* \equiv U\eta_x + V\eta_y + W\eta_z$, where $(\eta_x, \eta_y) = -(h_x, h_y)\eta_z$. Diffusion terms that feature the "artificial" viscosities or diffusivities (K_a^h, K_a^v) are considered unimportant, but retained (with small K_a^h, K_a^v) to help ensure numerical stability and convergence. A similar equation (not shown here) governs the other horizontal component V, while the true vertical velocity W is governed by

$$\frac{\partial}{\partial x}\left(\mathrm{UW} - K_a^h \frac{\partial W}{\partial x}\right) + \frac{\partial}{\partial y}\left(\mathrm{V\,W} - K_a^h \frac{\partial W}{\partial y}\right) + \frac{\partial}{\partial \eta}\left(W^* W - K_a^v \frac{\partial W}{\partial \eta}\right) = -\eta_z \frac{\partial P}{\partial \eta}. \tag{A.2}$$

The eddy viscosity is parameterized as

$$K = \lambda\sqrt{c_e E} = \frac{k_v \eta}{1 + k_v \eta/\lambda_0}\sqrt{c_e E} \tag{A.3}$$

where E is the turbulent kinetic energy (TKE); λ is the turbulence length scale, here prescribed such that at small heights η it reduces to $k_v\eta$ and for large height it approaches the constant limiting value λ_0 (here $\lambda_0 = 200$ m); and c_e is a closure constant representing the ratio u_*^2/E of the kinematic shear stress to the TKE in undisturbed, neutrally stratified flow. Finally the turbulent kinetic energy E is computed from

$$\begin{aligned} \frac{\partial}{\partial x}\left(\mathrm{U\,E} - K_a^h \frac{\partial E}{\partial x}\right) + \frac{\partial}{\partial y}\left(\mathrm{V\,E} - K_a^h \frac{\partial E}{\partial y}\right) + \frac{\partial}{\partial \eta}\left(W^* E - \eta_z^2 K \frac{\partial E}{\partial \eta}\right) \\ = K\left[\left(\eta_z \frac{\partial U}{\partial \eta}\right)^2 + \left(\eta_z \frac{\partial V}{\partial \eta}\right)^2\right] - \frac{(c_e E)^{3/2}}{\lambda}, \end{aligned} \tag{A.4}$$

where terms on the right hand side respectively represent shear production and viscous dissipation ("ϵ"), and are contrived to balance in the absence of any disturbance. These governing equations have been given in 'transport' (or 'flux') form, such that their left hand sides are the divergences of (the sum of) the advective and diffusive fluxes.

Further details

Vertical velocity was set to zero on ground, and at the top of the domain. The flow was driven by an imposed, laterally-invariant shear stress vector at the upper boundary ($\eta = D$), and a shallow constant stress layer was assumed to form beneath the lowest plane of gridpoints at $\eta = \eta_P$, such that the local velocities (U_P, V_P) determined the drag on ground (more detail is given by Wilson, 2018).

Except where otherwise specified, the constant c_e was evaluated on the assumption that in undisturbed and neutrally-stratified surface layer flow the normalized velocity standard deviations are $c_u = \sigma_u/u_* = 2$, $c_v = \sigma_v/u_* = 2$ and $c_w = \sigma_w/u_* = 1.3$ (with the implication that $c_e = 0.206$). However values of $\sigma_{u,v,w}/u_*$ given by the upwind sonic during intervals of south winds (that were not strongly stratified) were roughly (2.5, 2.5, 1.6), i.e. larger than those imposed in 'standard' simulations. This is not unduly surprising in view of some nearby irregularities of terrain and cover, and a simulation based on these larger values has also been shown (Figs. 10, 11).

The artificial viscosity (or diffusivity) for vertical diffusion K_a^v should be small relative to the true eddy viscosity, and accordingly was specified as $K_a^v = k_v u_* z_0/10 \sim 10^{-5}\,\mathrm{m^2\,s^{-1}}$; this ensured that (but for a small impact of the limiting length scale λ_0) the equilibrium wind profile $S_0(z)$ from ASL3D would be semi-logarithmic (see Fig. 5). The artificial diffusivity for horizontal diffusion was permitted to be larger, viz. $K_a^h = 10^{-1}\,\mathrm{m^2\,s^{-1}}$.

The vertical grid spacing $\Delta\eta$ was a constant $\Delta\eta = 10z_0$ below $\eta = 0.25$ m, and above that level $\Delta\eta$ was stretched by 20% for each layer in sequence up to a maximum allowed value, usually 30 m. For simulations shown, domain depth was $D = 360$ m or $D = 480$ m.

Non-linear terms in the equations, such as U^2, are (in effect) linearized by being expressed $U^{(m-1)}U^{(m)}$ as the product of a known value (the $m-1$th guess) and the sought for mth guess. Each solution step, $(m-1) \rightarrow (m)$, is known as an 'outer' iteration or cycle, and for the simulations shown $m \geq 2000$, ensuring convergence to a static solution. Even on the smallest domain, such simulations, performed on an Intel CORE i7 PC, took

of the order of hours to converge.

References

Bond, T.E., Laster, D.B., 1974. Influence of windbreaks on feedlot cattle in the Midwest. Trans. ASAE 17, 505–512.

Denmead, O.T., 1995. Novel meteorological methods for measuring trace gas fluxes. Philos. Trans. R. Soc. Lond. A 351, 383–396.

Dronen, S.I., 1988. Layout and design criteria for livestock windbreaks. Agric. Ecosyst. Environ. 22/23, 231–240.

Finnigan, J.J., Bradley, E.F., 1983. The turbulent kinetic energy budget behind a porous barrier: an analysis in streamline co-ordinates. J. Wind Eng. Ind. Aerodyn. 15, 157–168.

Hoerner, S.F., 1965. Fluid-Dynamic Drag. 455pp.

Jacobs, A.F.G., Wartena, L., 1987. Flow and turbulence around thin fences in perpendicular and oblique flow direction. Netherlands J. Agric. Sci. 35, 7–20.

Judd, M.J., Raupach, M.R., Finnigan, J.J., 1996. A wind tunnel study of turbulent flow around a single and multiple windbreaks. Part 1: Velocity fields. Boundary-Layer Meteorol. 80, 127–165.

Olsen, B.E., Wallander, R.T., 2002. Influence of winter weather and shelter on activity patterns of beef cows. Can. J. Anim. Sci. 82, 491–501.

Patton, E.G., Shaw, R.H., Judd, M.J., Raupach, M.R., 1998. Large-eddy simulation of windbreak flow. Boundary-Layer Meteorol. 87, 275–306.

Raine, J.K., Stevenson, D.C., 1977. Wind protection by model fences in a simulated atmospheric boundary layer. J. Ind. Aerodyn. 2, 159–180.

Wang, H., Takle, E.S., Shen, J., 2001. Shelterbelts and windbreaks: mathematical modeling and computer simulations of turbulent flows. Annu. Rev. Fluid Mech. 33, 549–586.

Wilson, J.D., 1985. Numerical studies of flow through a windbreak. J. Wind Eng. Ind. Aerodyn. 21, 119–154.

Wilson, J.D., 1987. On the choice of a windbreak porosity profile. Boundary-Layer Meteorol. 38, 37–49.

Wilson, J.D., 2004a. Oblique, stratified winds about a shelter fence, I: Measurements. J. Appl. Meteorol. 43, 1149–1167.

Wilson, J.D., 2004b. Oblique, stratified winds about a shelter fence, II: Comparison of measurements with numerical models. J. Appl. Meteorol. 43, 1392–1409.

Wilson, J.D., 2018. Measured and modelled wind variation over irregularly undulating terrain. Agric. For. Meteorol. 249, 187–197.

Wilson, J.D., Flesch, T.K., 2003. Wind measurements in a square plot enclosed by a shelter fence. Boundary-Layer Meteorol. 109, 191–224.

Wilson, J.D., Flesch, T.K., Crenna, B.P., et al., 2012. Estimating surface-air gas fluxes by inverse dispersion using a backward Lagrangian stochastic trajectory model. In: Lin, J. (Ed.), Lagrangian Modeling of the Atmosphere, Geophysical Monograph, No. 200. American Geophysical Union, pp. 149–161.